J Eng Math (2007) 59:61–82
DOI 10.1007/s10665-006-9074-x

ORIGINAL PAPER

Middle-field formulation for the computation of wave-drift loads

Xiao-Bo Chen

Received: 3 November 2005 / Accepted: 30 June 2006 / Published online: 27 September 2006

Abstract New formulations of second-order wave loads contributed by a first-order wave field are developed by applying two variants of Stokes's theorem and Gauss's theorem to a formulation consisting of direct pressure integrations on a body's hull which is called the near-field formulation. In addition to this direct formulation and the formulation derived from the momentum theorem called the far-field formulation, for the computation of drift (surge/sway) forces in horizontal directions and drift (yaw) moment around the vertical axis, one of new formulations is defined on the control surfaces surrounding the body and called the middle-field formulation. After a brief summary of both pressure-integration (near-field) and momentum (far-field) formulations, the development of the middle-field formulation involving control surfaces is described and complemented in detail in the appendices. The application of the new formulation shows that the near-field and far-field formulations are mathematically equivalent for wall-sided, as well as non-wall-sided bodies and under the condition that the mean yaw moments are expressed with respect to a space-fixed reference point. It is shown that the middle-field formulation is as robust as the far-field formulation and as general as the near-field formulation of second-order loads on a single body as well as on multiple bodies. Furthermore, the extension to the computation of a second-order oscillatory load, which is so far accessed only by the near-field formulation, is envisioned.

Keywords Far-field formulation · Middle-field formulation · Near-field formulation · Wave-drift load

1 Introduction

In offshore hydrodynamic applications, one key issue to the design of a mooring system is the accurate simulation of low-frequency motions in surge, sway and yaw of a system to which the second-order wave load is well known to be the main source of excitation. The development of new formulations for an accurate computation of second-order drift loads is presented here.

X.-B. Chen (✉)
Research Department, BUREAU VERITAS,
17bis, Place des Reflets, 92400 Courbevoie, France
e-mail: xiao-bo.chen@bureauveritas.com

Following this introduction the formulations of second-order wave loads are summarized. In particular, only the first-order wave field and the body's motion contribute to the second-order drift load, so that it can be directly evaluated, once the first-order solution is obtained. Two classes of formulations have been developed. One of these consists of direct pressure integrations on the hull of the body, as in [1–6], and is here called the near-field formulation. Another is derived in [7] and [8] by applying the momentum theorem to the fluid domain and is called the far-field formulation here. The near-field formulation is general, as it can be used to obtain all components of second-order wave loads applied to one individual body in a wave-body system of a single body or multiple bodies. On the other hand, the far-field formulation is restricted to give only three components, the *global* mean surge/sway forces and the mean yaw moments around the vertical axis applied to all bodies. However, the far-field formulation is preferred in practice whenever it is applicable owing to its numerical robustness as compared to the near-field formulation.

Since the starting points of the two formulations are so distinct that their representations are quite different, especially for floating bodies, additional terms associated with the body motion appear in the near-field formulation while the far-field formulation keeps the same form as for a fixed body without explicitly involving the body's motion. Having a common theoretical and rational basis, the equivalence of the two classical formulations is never put in doubt. However, numerical results in the literature are controversial as they give very close results in some cases and very different results in other cases. Especially for hulls that are non-wall-sided at the waterline, erroneous results, including positive surge forces in head waves of large periods, can be obtained by using the near-field formulation. As remarked in [9] most of results on wave-drift loads on a body with sharp corners using pressure integration (near-field formulation), show significant errors when compared with the far-field formulation. The direct connection between the two classical formulations has thus been an interesting issue.

Based on the use of two variants of Stokes's theorems given in [10] and presented in the appendices, it is shown mathematically that both formulations are indeed fully equivalent, regardless of the fact that the body hull is wall-sided or not, and under the condition that the reference point for mean yaw moments is space-fixed. This exercise, in addition, gives rise to several new formulations. A new near-field formulation is obtained by direct application of the variants of Stokes's theorem. It is essentially similar to the classical one with some improvements in the form of terms associated directly with the body's translations and rotations disappearing. Applying Gauss's theorem to the domain limited by a control surface, a second new formulation is obtained which involves integrals on the control surface and along its intersection with the mean free surface, and the part of free surface limited by the intersection and the waterline. An interesting feature of the formulation concerns the wave-drift loads for which the formulation is largely simplified. In particular, the horizontal components of drift loads involve only a surface integral on the control surface and a line integral along its intersection with the free surface. This formulation is defined on the control surface at some distance from the body is called the *middle-field* formulation.

Numerical results of second-order drift loads on a floating hemisphere, a Floating Production Storage Offloading (FPSO) unit and two bodies in side-by-side position, are presented. They confirm that the middle-field formulation has the same advantage as the far-field formulation, namely a rapid numerical convergence for horizontal drift loads (surge/sway forces and yaw moments). Furthermore, in the case of multiple bodies, the control surface can be one surrounding an individual body and the wave loads applied on the surrounded body are then obtained, while the far-field formulation provides only the sum of wave loads applied on all bodies.

By applying the momentum-conservation principle to a control fluid volume limited by the body hull, a control surface surrounding the body and the free surface in between, we obtain the same formulation as given in [6] and [11] which was written on the control surface for the components of the drift forces in the horizontal directions and the moment around the vertical axis. Unlike this local momentum analysis, the middle-field formulation presented here is directly derived from the near-field formulation, so that it provides a formal connection between the near-field and far-field formulations. Indeed, it is clarified that the usual far-field formulation is equivalent to the near-field formulation for bodies with a wall-sided, as

well as non-wall-sided hull and under the condition that the yaw moment is computed with respect to the space-fixed reference point. Furthermore, the new formulations are general and can be extended to the computation of the second-order loads occurring at the sum of wave frequencies as well as at the difference of wave frequencies, to horizontal load components as well as vertical load components, as envisioned in the discussion and conclusion.

2 Second-order wave loads contributed by the first-order wave field

We consider bodies floating on a free surface in the presence of incident propagating waves. A reference system in Cartesian coordinates is defined by letting the (x, y)-plane coincide with the mean free surface and the z-axis is positive upwards so that

$$z = \eta(x, y, t) \tag{1}$$

describes the elevation of free surface.

The fluid is assumed to be incompressible and inviscid and the fluid motion is irrotational. Under these assumptions of a perfect fluid, the flow velocity $\mathbf{V} = (V_1, V_2, V_3)$ can be expressed as the gradient of a scalar potential $\Phi(x, y, z, t)$ in the space (x, y, z) at the time t as $\mathbf{V} = \nabla\Phi$. The velocity potential satisfies the Laplace equation:

$$\nabla^2\Phi = 0, \tag{2}$$

which becomes the governing equation in the fluid domain.

2.1 First-order wave fields

By assuming small steepness of the incoming waves and small magnitude of the motions of the floating bodies around their mean positions, the velocity potential can be expanded in a series of different orders with respect to the wave steepness. At the first-order, the velocity potential satisfies the linearized condition on the mean free surface $F(z = 0)$:

$$g\Phi_z + \Phi_{tt} = 0 \tag{3}$$

with g the acceleration due to gravity, $\Phi_z = \partial\Phi/\partial z$ and $\Phi_{tt} = \partial^2\Phi/\partial t^2$, and the boundary condition on the hull H:

$$\Phi_n = \mathbf{X}_t \cdot \mathbf{n} \tag{4}$$

where $\Phi_n = \partial\Phi/\partial n$ and $\mathbf{X}_t = \partial\mathbf{X}/\partial t$ with $\mathbf{X} = (\zeta_1, \zeta_2, \zeta_3)$ representing the vector describing body displacement associated with its motion composed of translations and rotations.

Together with the condition $\Phi_z = 0$ on the sea bed $B(z = -h)$ and the radiation condition $\Phi \to \Phi_\mathrm{I}$ (with Φ_I being the known velocity potential of incoming waves) on a control surface $S_\infty(R = \sqrt{x^2 + y^2} \to \infty)$ at infinity, the Laplace equation (2), and the boundary conditions on the mean free surface (3) and on the hull (4) compose a boundary-value problem describing wave–body interactions. The system (2–4) of wave diffraction and radiation around bodies can be solved by applying the method of boundary-integral equations. In this method, the velocity potential is decomposed as

$$\Phi = \Phi_\mathrm{I} + \Phi_\mathrm{P}, \tag{5}$$

which is the sum of the known potential Φ_I representing incoming waves and the perturbation potential Φ_P due to the presence of bodies (which can be further written as $\Phi_\mathrm{P} = \Phi_\mathrm{D} + \Phi_\mathrm{R}$ the sum of diffraction and radiation components). In the frequency domain, the velocity potentials (as well as all other variables) are written as the real part of the product of the complex function in space and harmonic function in time:

$$(\Phi, \Phi_\mathrm{I}, \Phi_\mathrm{P}, \mathbf{X}) = \mathfrak{Re}\{(\phi, \phi_\mathrm{I}, \phi_\mathrm{P}, \mathbf{x})\mathrm{e}^{-\mathrm{i}\omega t}\} \tag{6}$$

with ω being the wave frequency and $\mathfrak{Re}\{\cdot\}$ representing the real part. The potential ϕ_{I} of the incoming waves is written as

$$\phi_{\mathrm{I}} = -\frac{ag}{\omega}\frac{\cosh[k(z+h)]}{\cosh(kh)}\mathrm{e}^{\mathrm{i}k(x\cos\beta+y\sin\beta)} \tag{7}$$

where (a, β, h) are wave amplitude, heading and waterdepth, respectively. The wavenumber k is determined by the dispersion equation $\omega^2 = gk\tanh(kh)$.

Based on the source distribution $\sigma(Q)$ on hull H, the perturbation potential and its gradient are expressed by

$$\phi_{\mathrm{P}}(P) = \iint_H \mathrm{d}s\,\sigma(Q)G(P,Q) \quad \text{and} \quad \nabla\phi_{\mathrm{P}}(P) = \iint_H \mathrm{d}s\,\sigma(Q)\nabla G(P,Q) \tag{8}$$

with $Q \subset H$. The Green function $G(P,Q)$ in (8), representing a potential flow at a field point P generated by a point source located at Q, satisfies $\nabla^2 G(P,Q) = 4\pi\delta(P-Q)$ in the fluid domain and the same conditions as Φ on all boundaries, except of that on the hull on which we have the integral equation

$$2\pi\sigma(P) + \iint_H \mathrm{d}s\,\sigma(Q)G_n(P,Q) = -\mathbf{n}\cdot\nabla\phi_{\mathrm{I}} - \mathrm{i}\omega\mathbf{x}\cdot\mathbf{n} \tag{9}$$

to determine the source distribution $\sigma(Q)$. Extensive studies on $G(P,Q)$ can be found in [12–14]. Once the solution has been found, the velocity potential and its gradient are obtained by (8) as well as the free-surface elevation by

$$\eta = -\Phi_t/g \tag{10}$$

evaluated at $z = 0$.

At a point $P(z, R, \theta)$ of large horizontal distance from bodies ($R \to \infty$), the perturbation potential is expressed asymptotically in [15] by

$$\phi_{\mathrm{P}}(z,R,\theta) = -\sqrt{\frac{8\pi k}{R}}\frac{2\sinh^2(kh)}{2kh+\sinh(2kh)}\frac{\cosh[k(z+h)]}{\sinh(kh)}K(\theta)\mathrm{e}^{\mathrm{i}(kR+\pi/4)} \tag{11}$$

in which $K(\theta)$ is the Kochin function defined by

$$K(\theta) = \iint_H \mathrm{d}s\,\sigma(Q)\frac{\cosh[k(z'+h)]}{\sinh(kh)}\mathrm{e}^{-\mathrm{i}k(x'\cos\theta+y'\sin\theta)} \quad \text{with} \quad Q(x',y',z') \subset H \tag{12}$$

which is used in the far-field formulation of wave-drift loads.

2.2 Classical near-field formulation of second-order loads

Numerous studies have been devoted to the analysis of second-order wave loads. A non-exhaustive list includes the following classical work [1–8]. A general formulation of second-order wave loads can be obtained by direct integration of the second-order pressure on the hull surface of the body's *mean* position; the first-order pressure in the intermittent zone around the waterline and the variation of the first-order loads are due to first-order motions. The second-order wave load $(\mathbf{F}_T, \mathbf{M}_T)$ is then composed of one part $(\mathbf{F}_1, \mathbf{M}_1)$ dependent on the quadratic product of the first-order quantities and another part $(\mathbf{F}_2, \mathbf{M}_2)$ contributed by the second-order potentials.

$$(\mathbf{F}_T, \mathbf{M}_T) = (\mathbf{F}_1, \mathbf{M}_1) + (\mathbf{F}_2, \mathbf{M}_2) \tag{13}$$

As we are mostly interested here in the wave-drift load which is not contributed by the second-order time-harmonic potential, we represent the second-order wave load only by its first part:

$$(\mathbf{F}_1, \mathbf{M}_1) = (\mathbf{F}, \mathbf{M}) + (\mathbf{F}_S, \mathbf{M}_S) \tag{14}$$

where $\mathbf{F} = (F^x, F^y, F^z)$ stands for the forces and $\mathbf{M} = (M^x, M^y, M^z)$ for the moments. $(\mathbf{F}_S, \mathbf{M}_S)$ are the second-order variation of the hydrostatic loads due to the first-order motions as defined in [6], which give only non-zero values for the vertical force and moments around the horizontal axes. Furthermore, since $(\mathbf{F}_S, \mathbf{M}_S)$ depend only on the hull geometry and first-order motions, they can be evaluated without any numerical difficulty. Thus, in the following, we will concentrate on $(\mathbf{F}, \mathbf{M})$ which is given in [5] by

$$\mathbf{F} = \rho \iint_H \mathrm{d}s \left[\frac{(\nabla\Phi)^2}{2} + \mathbf{X}\cdot\nabla\Phi_t + \Phi_t \mathbf{R}\wedge \right]\mathbf{n} + \frac{\rho g}{2}\oint_\Gamma \mathrm{d}\ell\, \eta(2\zeta_3 - \eta)\mathbf{n}, \tag{15}$$

$$\mathbf{M} = \rho \iint_H \mathrm{d}s \left\{ \left[\frac{(\nabla\Phi)^2}{2} + \mathbf{X}\cdot\nabla\Phi_t + \Phi_t \mathbf{R}\wedge \right](\mathbf{r}\wedge\mathbf{n}) + \Phi_t \mathbf{T}\wedge\mathbf{n} \right\} + \frac{\rho g}{2}\oint_\Gamma \mathrm{d}\ell\, \eta(2\zeta_3 - \eta)(\mathbf{r}\wedge\mathbf{n}), \tag{16}$$

in which all involved quantities in the integrand are of the *first order* in η for the free-surface elevation defined by (10), Φ for the velocity potential defined by (5–8), $\mathbf{X} = \mathbf{T} + \mathbf{R}\wedge\mathbf{r} = (\zeta_1, \zeta_2, \zeta_3)$ for the displacement due to the translation $\mathbf{T} = (\xi_1, \xi_2, \xi_3)$ and rotation $\mathbf{R} = (\theta_1, \theta_2, \theta_3)$, and $\mathbf{r} = (x - x_0, y - y_0, z - z_0)$ for the position vector with respect to the reference point (x_0, y_0, z_0) of rotation. In (15, 16), Γ stands for the intersection (waterline) of the hull H at its mean position with the mean free surface $F(z = 0)$. The normal vector $\mathbf{n} = (n_1, n_2, n_3)$ is positively oriented inwards with respect to the fluid. The vector $\mathbf{r}\wedge\mathbf{n} = (n_4, n_5, n_6)$ is also used in the following.

The first term in the hull integral of (15, 16) comes directly from the convective term in Bernoulli's equation, while the second term is the correction of the first-order dynamic pressure with respect to the displacement. The term associated with the rotation $\mathbf{R}$ takes into account the variation of the normal vector. Finally, the last term in the hull integral of (16) is the additional moment with respect to the space-fixed reference point, induced by the first-order dynamic load applied to the instantaneous reference point translated due to the motion of the body. This term was omitted in [1, 4] and [6] as it is understood that the moment is evaluated with respect to the body-fixed reference point. Other terms in (15, 16) show a difference of higher order between their values with respect the body-fixed reference point and that with respect to the space-fixed reference point.

The line integral in (15, 16) is the result of the integration of the first-order pressure on the intermittent zone around the waterline of a wall-sided body. The integrand of the waterline integral is also used in [6] but different from that in [1] and [4]. It is shown in [5] that the two expressions of the second-order loads are equivalent.

At the waterline, the angle γ between the normal vector $\mathbf{n}$ and the horizontal plane in the near-field formulation (15, 16), is assumed to be zero, i.e., the hull intersects the mean free surface vertically. If the hull is not wall-sided ($\gamma \neq 0$), the relative waterline integral in [2, 3] and [6] is raised by the factor $1/|\cos\gamma|$ which takes account of the increase of the intermittent surface due to a relative wave elevation along the waterline. This implies that we have to modify the normal vector $\mathbf{n}$ into $\mathbf{n}' = \mathbf{n}/|\cos\gamma|$ in the waterline integral of (15, 16). Here we adopt the expression given in [6]:

$$\mathbf{F} = \rho \iint_H \mathrm{d}s \left[\frac{(\nabla\Phi)^2}{2} + \mathbf{X}\cdot\nabla\Phi_t + \Phi_t \mathbf{R}\wedge \right]\mathbf{n} + \frac{\rho g}{2}\oint_\Gamma \mathrm{d}\ell\, \eta(2\zeta_3 - \eta)\mathbf{n}', \tag{17}$$

$$\mathbf{M} = \rho \iint_H \mathrm{d}s \left\{ \left[\frac{(\nabla\Phi)^2}{2} + \mathbf{X}\cdot\nabla\Phi_t + \Phi_t \mathbf{R}\wedge \right](\mathbf{r}\wedge\mathbf{n}) + \Phi_t \mathbf{T}\wedge\mathbf{n} \right\} + \frac{\rho g}{2}\oint_\Gamma \mathrm{d}\ell\, \eta(2\zeta_3 - \eta)(\mathbf{r}\wedge\mathbf{n}'), \tag{18}$$

with $\mathbf{n}' = \mathbf{n}/|\cos\gamma|$ and the last term in the hull integral of (18) as the additional moment with respect to the space-fixed reference point.

Expressions (17, 18) involving the body's response $(\mathbf{T}, \mathbf{R})$ and the first-order wave field (velocity potential Φ, its gradient $\nabla\Phi$ and wave elevation η) on the hull H and along the waterline Γ, is called here the *near-field* formulation. It includes all components of wave loads oscillating at the sum of wave frequencies as well as the difference of wave frequencies. In particular, the wave-drift load in regular waves is obtained by taking the mean value during one wave period.

2.3 Classical far-field formulation of wave-drift loads

By applying the conservation principle of linear and angular momentum to the fluid domain bounded by the body surface H, the free surface F and a control surface S_∞ at infinity, Newman [8] extended Maruo's formulation [7] for the horizontal drift forces to all three components, including the moment around the vertical axis. The momentum formulation equivalent to that given in [8] is written as:

$$F_D^x = \left\langle \frac{\rho g}{2} \int_{\Gamma_\infty} \mathrm{d}l\, \eta^2 n_1 + \iint_{S_\infty} \mathrm{d}s\, (\rho \Phi_n \Phi_x + P n_1) \right\rangle \tag{19}$$

$$F_D^y = \left\langle \frac{\rho g}{2} \int_{\Gamma_\infty} \mathrm{d}l\, \eta^2 n_2 + \iint_{S_\infty} \mathrm{d}s\, (\rho \Phi_n \Phi_y + P n_2) \right\rangle \tag{20}$$

$$M_D^z = \left\langle \frac{\rho g}{2} \int_{\Gamma_\infty} \mathrm{d}l\, \eta^2 n_6 + \iint_{S_\infty} \mathrm{d}s \left\{ \rho \Phi_n [(x - x_0)\Phi_y - (y - y_0)\Phi_x] + P n_6 \right\} \right\rangle \tag{21}$$

written on a surface S_∞ located at infinity and the upper boundary Γ_∞ touching vertically the mean free surface. The pressure in (19–21) is given by $P = -\rho(\Phi_t + \nabla\Phi \cdot \nabla\Phi/2 + gz)$. The symbol "$\langle\cdot\rangle$" stands for taking the average value during one period. The line integral along Γ_∞ in (19–21) is the resultant from the pressure integral between the mean and instantaneous positions of the free surface included in the compact form of the control-surface integral (Equations 14–16) in [8]. On the control surface S_∞ and along Γ_∞, asymptotic expressions (11) of Φ_P, as well as the wave elevation η (10) involving the Kochin function $K(\theta)$ given by (12), can be introduced into (19–21) which becomes a single integral of the polar variable after analytical integration in the vertical direction. The general expressions given in [15] are reported below:

$$F_D^x = -4\pi\rho \frac{k^2 \sinh^2(kh)}{2kh + \sinh(2kh)} \int_0^{2\pi} |K(\theta)|^2 \cos\theta \,\mathrm{d}\theta - 2\pi\rho a\omega \Im\mathrm{m}\{K(\beta)\} \cos\beta, \tag{22}$$

$$F_D^y = -4\pi\rho \frac{k^2 \sinh^2(kh)}{2kh + \sinh(2kh)} \int_0^{2\pi} |K(\theta)|^2 \sin\theta \,\mathrm{d}\theta - 2\pi\rho a\omega \Im\mathrm{m}\{K(\beta)\} \sin\beta, \tag{23}$$

$$M_D^z = -4\pi\rho \frac{k \sinh^2(kh)}{2kh + \sinh(2kh)} \int_0^{2\pi} \Im\mathrm{m}\{\bar{K}(\theta) K'(\theta)\} \mathrm{d}\theta + 2\pi\rho a\omega \Re\mathrm{e}\{K'(\beta)\}/k, \tag{24}$$

where $\bar{K}(\theta)$ and $K'(\theta)$ are the complex conjugates of the Kochin function defined by (12) and its derivative with respect to θ, respectively. $\Re\mathrm{e}\{\cdot\}$ and $\Im\mathrm{m}\{\cdot\}$ stand for the real and imaginary parts, respectively. The formulations (22–24) are developed for finite waterdepth. For the case of deep water, the expressions (22–24) for $h \to \infty$ become equivalent to those given in [8].

This far-field formulation (22–24) gives the three components of the global wave-drift load. It is numerically robust, since the Kochin function $K(\theta)$ and its derivative $K'(\theta)$ are far less sensitive to the discretisation of the hull. On the other hand, the near-field formulation (17, 18) provides all components of wave loads on an individual body but it suffers from poor convergence, as singularities are present in the velocity field around the hull area with a sharp variation of geometry at corners. Theoretically, both the near-field and far-field formulations must yield the same result for the three components of the wave-drift loads.

3 New formulations of second-order wave loads

Comparing both the near-field formulation (17, 18) and the far-field formulation (19–21), the most striking difference is the involvement of the body motions $(\mathbf{T}, \mathbf{R})$ in (17, 18). To make the connection between both, the terms involving $(\mathbf{T}, \mathbf{R})$ can be treated as a starting point. Indeed, we have started to develop a new near-field formulation by applying variants of Stokes's theorem. Considering a fluid volume enclosed

by the hull, a control surface at a distance from the body and the mean free surface limited by the waterline and the intersection of the control surface with the free surface, we obtain a general formulation of second-order loads by using Gauss's theorem. Finally, the middle-field formulation written only on the control surface is obtained for the computation of wave-drift loads.

3.1 New near-field formulation

We consider the two variants of Stokes's theorem (49) and (53) given as Equations (1.3.5) and (1.3.13) in [10] which are also developed here in Appendix A. Introducing the identity $\mathbf{A} = (\Phi_t \mathbf{X})$ into (49) and (53), we have the following two identities:

$$\rho \iint_H \mathrm{d}s\, (\mathbf{X}\cdot\nabla\Phi_t)\mathbf{n} = \rho \iint_H \mathrm{d}s \left[\nabla\Phi_t(\mathbf{X}\cdot\mathbf{n}) - \mathbf{R}\wedge(\Phi_t\mathbf{n})\right] - \rho g \oint_\Gamma \mathrm{d}\ell\, \eta\left[\zeta_3\bar{\mathbf{n}} - (\mathbf{X}\cdot\bar{\mathbf{n}})\mathbf{k}\right], \tag{25}$$

$$\begin{aligned}\rho \iint_H \mathrm{d}s\, (\mathbf{X}\cdot\nabla\Phi_t)(\mathbf{r}\wedge\mathbf{n}) &= \rho \iint_H \mathrm{d}s \Big[(\mathbf{r}\wedge\nabla\Phi_t)(\mathbf{X}\cdot\mathbf{n}) - \Phi_t\mathbf{T}\wedge\mathbf{n} - \mathbf{R}\wedge(\mathbf{r}\wedge\mathbf{n})\Phi_t\Big] \\ &\quad - \rho g \oint_\Gamma \mathrm{d}\ell\, \eta[\zeta_3(\mathbf{r}\wedge\bar{\mathbf{n}}) - (\mathbf{X}\cdot\bar{\mathbf{n}})(\mathbf{r}\wedge\mathbf{k})],\end{aligned} \tag{26}$$

respectively. The normal vector $\bar{\mathbf{n}}$ in the waterline integral is given on the mean free surface, $\bar{\mathbf{n}} = \mathbf{n}$ for a wall-sided hull. In general, $\bar{\mathbf{n}} = (n_1, n_2, 0)/|\cos\gamma|$ with γ the angle between $\mathbf{n}$ and the horizontal plane as noted in the development of the above identities (25, 26) which is detailed in Appendix B. It should be noted that $\bar{\mathbf{n}}$ is different from $\mathbf{n}'$ used in [2, 3] and [6] for the vertical component, since $\mathbf{n}'$ is not given on the mean free surface if $\gamma \neq 0$ as $\mathbf{n}' = \mathbf{n}/|\cos\gamma| = \bar{\mathbf{n}} + (0, 0, n_3)/|\cos\gamma|$.

Introducing (25, 26) into the near-field formulation (17, 18), we obtain a new near-field formulation:

$$\mathbf{F} = \rho \iint_H \mathrm{d}s \left[\frac{(\nabla\Phi)^2}{2}\mathbf{n} + \nabla\Phi_t(\mathbf{X}\cdot\mathbf{n})\right] - \frac{\rho g}{2}\oint_\Gamma \mathrm{d}\ell \left[\eta^2\bar{\mathbf{n}} + \Xi\,\mathbf{k}\right], \tag{27}$$

$$\mathbf{M} = \rho \iint_H \mathrm{d}s \left[\frac{(\nabla\Phi)^2}{2}(\mathbf{r}\wedge\mathbf{n}) + (\mathbf{r}\wedge\nabla\Phi_t)(\mathbf{X}\cdot\mathbf{n})\right] - \frac{\rho g}{2}\oint_\Gamma \mathrm{d}\ell \left[\eta^2(\mathbf{r}\wedge\bar{\mathbf{n}}) + \Xi(\mathbf{r}\wedge\mathbf{k})\right] \tag{28}$$

with Ξ defined by

$$\Xi = (\eta^2 - 2\eta\zeta_3)n_3/|\cos\gamma| - 2\eta(\mathbf{X}\cdot\bar{\mathbf{n}}),$$

which is involved in the waterline integral giving only a contribution to the vertical forces and moments around the horizontal axes. For a wall-sided hull, $n_3 = 0$ so that $\Xi = -2\eta(\mathbf{X}\cdot\mathbf{n})$.

The above formulation (27, 28) is essentially similar to (17, 18) with some interesting improvements such as that all terms with body motion $(\mathbf{T}, \mathbf{R})$ disappear, as expected, and the term involving the displacement in the waterline integral gives a contribution only to the vertical components.

3.2 New formulations involving control surfaces

Now we consider a domain D surrounded by $S = H \cup C \cup F$ with the body hull H at its mean position, a fictitious (control) surface C surrounding the body and the mean free surface F limited by the intersection Γ of H with $z = 0$ and that Γ_c of C with $z = 0$, as shown in Fig. 12. Applying Gauss's formula (65) and (68) shown in Appendix C, we develop the hull integral in (27, 28) as:

$$\begin{aligned}\iint_H \mathrm{d}s \left[\frac{(\nabla\Phi)^2}{2}\mathbf{n} + \nabla\Phi_t(\mathbf{X}\cdot\mathbf{n})\right] &= \iint_H \mathrm{d}s \left[\Phi_n\nabla\Phi + \nabla\Phi_t(\mathbf{X}\cdot\mathbf{n})\right] \\ &\quad + \iint_F \mathrm{d}s \left[\Phi_n\nabla\Phi - \frac{(\nabla\Phi)^2}{2}\mathbf{n}\right] + \iint_C \mathrm{d}s \left[\Phi_n\nabla\Phi - \frac{(\nabla\Phi)^2}{2}\mathbf{n}\right],\end{aligned} \tag{29}$$

$$\iint_H \mathrm{d}s \left[\frac{(\nabla\Phi)^2}{2}(\mathbf{r}\wedge\mathbf{n}) + (\mathbf{r}\wedge\nabla\Phi_t)(\mathbf{X}\cdot\mathbf{n})\right] = \iint_H \mathrm{d}s \left[\Phi_n(\mathbf{r}\wedge\nabla\Phi) + (\mathbf{r}\wedge\nabla\Phi_t)(\mathbf{X}\cdot\mathbf{n})\right] + \iint_F \mathrm{d}s \left[\Phi_n(\mathbf{r}\wedge\nabla\Phi) - \frac{(\nabla\Phi)^2}{2}(\mathbf{r}\wedge\mathbf{n})\right] + \iint_C \mathrm{d}s \left[\Phi_n(\mathbf{r}\wedge\nabla\Phi) - \frac{(\nabla\Phi)^2}{2}(\mathbf{r}\wedge\mathbf{n})\right]. \tag{30}$$

By making use of above identities (29, 30) in (27, 28), we obtain:

$$\mathbf{F} = \rho\iint_H \mathrm{d}s\left[\Phi_n\nabla\Phi + \nabla\Phi_t(\mathbf{X}\cdot\mathbf{n})\right] - \frac{\rho g}{2}\oint_\Gamma \mathrm{d}\ell\left[\eta^2\bar{\mathbf{n}} + \Xi\,\mathbf{k}\right] + \frac{\rho}{2}\iint_F \mathrm{d}s\left[2\Phi_n\nabla\Phi - (\nabla\Phi)^2\mathbf{n}\right] + \frac{\rho}{2}\iint_C \mathrm{d}s\left[2\Phi_n\nabla\Phi - (\nabla\Phi)^2\mathbf{n}\right], \tag{31}$$

$$\mathbf{M} = \rho\iint_H \mathrm{d}s\,\mathbf{r}\wedge\left[\Phi_n\nabla\Phi + \nabla\Phi_t(\mathbf{X}\cdot\mathbf{n})\right] - \frac{\rho g}{2}\oint_\Gamma \mathrm{d}\ell\left[\eta^2(\mathbf{r}\wedge\bar{\mathbf{n}}) + \Xi(\mathbf{r}\wedge\mathbf{k})\right] + \frac{\rho}{2}\iint_F \mathrm{d}s\,\mathbf{r}\wedge\left[2\Phi_n\nabla\Phi - (\nabla\Phi)^2\mathbf{n}\right] + \frac{\rho}{2}\iint_C \mathrm{d}s\,\mathbf{r}\wedge\left[2\Phi_n\nabla\Phi - (\nabla\Phi)^2\mathbf{n}\right]. \tag{32}$$

Over the free surface F and along the waterline Γ of body and Γ_c of the control surface, we have $\Phi_t = -g\eta$ from (10) so that the identities (69) and (70) can be rewritten as:

$$-g\oint_\Gamma \mathrm{d}\ell\,\eta^2\bar{\mathbf{n}} = 2\iint_F \mathrm{d}s\,\eta(\Phi_{zt}\mathbf{k} - \nabla\Phi_t) + g\oint_{\Gamma_c} \mathrm{d}\ell\,\eta^2\bar{\mathbf{n}}, \tag{33}$$

$$-g\oint_\Gamma \mathrm{d}\ell\,\eta^2(\mathbf{r}\wedge\bar{\mathbf{n}}) = 2\iint_F \mathrm{d}s\,\eta\left[\Phi_{zt}(\mathbf{r}\wedge\mathbf{k}) - \mathbf{r}\wedge\nabla\Phi_t\right] + g\oint_{\Gamma_c} \mathrm{d}\ell\,\eta^2(\mathbf{r}\wedge\bar{\mathbf{n}}) \tag{34}$$

derived from the application of Gauss's integral for the plane as developed in Appendix C. Introducing above identity (33, 34) into (31, 32), we obtain the new formulation:

$$\mathbf{F} = \rho\iint_H \mathrm{d}s\left[\nabla\Phi(\mathbf{X}_t\mathbf{n}) + \nabla\Phi_t(\mathbf{X}\cdot\mathbf{n})\right] - \frac{\rho g}{2}\oint_\Gamma \mathrm{d}\ell\,\Xi\,\mathbf{k} - \rho\iint_F \mathrm{d}s\left[(\Phi_z\nabla\Phi + \eta\nabla\Phi_t) - (\eta\Phi_{zt} + \nabla\Phi\nabla\Phi/2)\mathbf{k}\right] + \frac{\rho g}{2}\oint_{\Gamma_c} \mathrm{d}\ell\,\eta^2\mathbf{n} + \frac{\rho}{2}\iint_C \mathrm{d}s\left[2\Phi_n\nabla\Phi - (\nabla\Phi)^2\mathbf{n}\right], \tag{35}$$

$$\mathbf{M} = \rho\iint_H \mathrm{d}s\,\mathbf{r}\wedge\left[\nabla\Phi(\mathbf{X}_t\cdot\mathbf{n}) + \nabla\Phi_t(\mathbf{X}\cdot\mathbf{n})\right] - \frac{\rho g}{2}\oint_\Gamma \mathrm{d}\ell\,\Xi(\mathbf{r}\wedge\mathbf{k}) - \rho\iint_F \mathrm{d}s\left[\mathbf{r}\wedge(\Phi_z\nabla\Phi + \eta\nabla\Phi_t) - (\eta\Phi_{zt} + \nabla\Phi\nabla\Phi/2)(\mathbf{r}\wedge\mathbf{k})\right] + \frac{\rho g}{2}\oint_{\Gamma_c} \mathrm{d}\ell\,\eta^2(\mathbf{r}\wedge\mathbf{n}) + \frac{\rho}{2}\iint_C \mathrm{d}s\left[2\Phi_n(\mathbf{r}\wedge\nabla\Phi) - (\nabla\Phi)^2(\mathbf{r}\wedge\mathbf{n})\right]. \tag{36}$$

The new formulation (35, 36) is general as it applies to all components of second-order wave loads contributed by the first-order wave field, including high-frequency loads (second-order loads occurring at the frequency equal to the sum of wave frequencies), as well as the low-frequency loads (second-order loads occurring at a frequency equal to the difference of wave frequencies), to horizontal and vertical load components. The control surface C can be at a finite distance from the body or one pushed to infinity. In the first case, C may be pushed back to H while, in the second case, C may be composed of the surface of a vertical cylinder plus the seabed. Furthermore, in the case of multiple bodies, the control surface C can be one surrounding an individual body and (35, 36) gives the wave loads applied on the surrounded body.

3.3 Middle-field formulation of wave drift loads

An interesting feature of (35, 36) concerns the wave-drift load for which the formulation is greatly simplified. It can be easily checked that the hull integral gives zero contribution, since the integrand can be

grouped as $\partial[\nabla\Phi(\mathbf{X}\cdot\mathbf{n})]/\partial t$ which has zero mean in one period. The same is true for the first term in the integral over the limited region of the free surface, as $\Phi_z = \eta_t$ from the boundary condition on the free surface. The formulation (35, 36) can be rewritten as:

$$\mathbf{F}_D = \left\langle -\frac{\rho g}{2}\oint_\Gamma \mathrm{d}\ell\, \Xi\,\mathbf{k} + \rho\iint_F \mathrm{d}s\,(\eta\Phi_{zt} + \nabla\Phi\cdot\nabla\Phi/2)\mathbf{k} + \frac{\rho g}{2}\oint_{\Gamma_c}\mathrm{d}\ell\,\eta^2\bar{\mathbf{n}} + \frac{\rho}{2}\iint_C \mathrm{d}s\left[2\Phi_n\nabla\Phi - (\nabla\Phi\cdot\nabla\Phi)\mathbf{n}\right]\right\rangle, \tag{37}$$

$$\mathbf{M}_D = \left\langle -\frac{\rho g}{2}\oint_\Gamma \mathrm{d}\ell\, \Xi(\mathbf{r}\wedge\mathbf{k}) + \rho\iint_F \mathrm{d}s\,(\eta\Phi_{zt} + \nabla\Phi\cdot\nabla\Phi/2)(\mathbf{r}\wedge\mathbf{k}) + \frac{\rho g}{2}\oint_{\Gamma_c}\mathrm{d}\ell\,\eta^2\mathbf{r}\wedge\bar{\mathbf{n}} + \frac{\rho}{2}\iint_C \mathrm{d}s\left[2\Phi_n(\mathbf{r}\wedge\nabla\Phi) - (\nabla\Phi\cdot\nabla\Phi)(\mathbf{r}\wedge\mathbf{n})\right]\right\rangle \tag{38}$$

for all components of drift loads on one body surrounded by the control surface. The waterline integral and the free-surface integral in (37, 38) give only contributions to the vertical force and the moments around the horizontal axes. The horizontal forces and moment around the vertical axis are thus given by the integral on the control surface C and along its intersection Γ_c only:

$$F_D^x = \left\langle \frac{\rho g}{2}\oint_{\Gamma_c}\mathrm{d}\ell\,\eta^2\,\bar{n}_1 + \rho\iint_C \mathrm{d}s\left[\Phi_n\Phi_x - (\nabla\Phi\cdot\nabla\Phi/2)\,n_1\right]\right\rangle \tag{39}$$

$$F_D^y = \left\langle \frac{\rho g}{2}\oint_{\Gamma_c}\mathrm{d}\ell\,\eta^2\,\bar{n}_2 + \rho\iint_C \mathrm{d}s\left[\Phi_n\Phi_y - (\nabla\Phi\cdot\nabla\Phi/2)\,n_2\right]\right\rangle \tag{40}$$

$$M_D^z = \left\langle \frac{\rho g}{2}\oint_{\Gamma_c}\mathrm{d}\ell\,\eta^2\,\bar{n}_6 + \rho\iint_C \mathrm{d}s\left\{\Phi_n\left[(x-x_0)\Phi_y - (y-y_0)\Phi_x\right] - (\nabla\Phi\cdot\nabla\Phi/2)\,n_6\right\}\right\rangle \tag{41}$$

The new formulation (39–41) for the computation of the three components of drift loads written on the control surface at a certain distance from one body is the called *middle-field* formulation. This formulation is confirmed by the fact that it is equivalent to that obtained in [6] and [11] by applying the momentum-conservation principle to a control fluid volume limited by the body hull, a control surface and the free surface in between. If the control surface C is moved to infinity as S_∞ which intersects vertically the mean free surface, we have $(\bar{n}_2, \bar{n}_2, \bar{n}_6) = (n_1, n_2, n_6)$ since $\bar{\mathbf{n}} = \mathbf{n}$ and $\mathbf{r}\wedge\bar{\mathbf{n}} = \mathbf{r}\wedge\mathbf{n}$, and the expression (39–41) is in full agreement with (19–21) as Γ_c becomes Γ_∞ and $\langle P\rangle = -\langle\nabla\Phi\cdot\nabla\Phi/2\rangle$ on S_∞. Due to the fact that (39–41) is derived from the near-field formulation by using the variants of Stokes's and Gauss's theorem, its connection with the far-field formulation (22–24) through (19–21) obtained by applying the momentum theorem shows formally that both the near-field (17, 18) and far-field formulation (22–24) are indeed equivalent for the horizontal drift forces and moment around the vertical axis, for wall-sided as well as non-wall-sided bodies.

If the control surface C is allowed to coincide with H, we find the same result as that in [6] which is derived by making use of the momentum theorem. However, there is not any advantage compared to the original (17, 18) or the new one (27, 28), since the gradient of the velocity potential present in these formulations converges slowly at the hull.

Unlike these two particular cases, the control surface C can be one at a distance from the body where the wave field, in particular, the gradient of the velocity potential is not greatly affected by the degree of accuracy in the description of the hull geometry. The distance may not be very far. In general, a distance equal to the size of several panels is sufficient. The middle-field formulation written on the control surface gives results of excellent convergence. Furthermore, the form of the control surface is arbitrary so that the most convenient form, such as a parallelepiped surface or an ellipsoidal surface surrounding the body, can be generated automatically.

4 Numerical results

Three numerical examples are presented here. Different formulations are compared for the case of a free floating hemisphere of radius R in deep water. A study of the numerical convergence of wave-drift loads using the near-field, far-field and middle-field formulations is carried out for a FPSO. The middle-field formulation (39–41) is applied to the case of a barge and a Wigley hull in side-by-side position. The numerical results are then compared with measurements.

4.1 Floating hemisphere

In Fig. 1, the mesh of a hemisphere of radius R with 390 panels on one quarter of the hull and a control surface of size ($L_c \times B_c \times D_c = 2.2R \times 2.2R \times 1.1R$) is illustrated. The drift forces $F_D^x/(\rho g R a^2/2)$ with a being the amplitude of the incoming waves obtained by different formulations are presented in Fig. 2 against the wavenumber (kR). The results for the new near-field formulation (27, 28) are exactly the same as those of the classical near-field formulation (17, 18), as shown mathematically. As expected, the results obtained by using the middle-field formulation (39–41) are very close to those resulting from the classical far-field formulation (22–24). The difference between the near-field formulation and the middle-field formulation or the far-field formulation has to do with the mesh fineness. The asymptotic value of the horizontal drift force $F_D^x/(\rho g R a^2/2) \to 4/3$ when $kR \to \infty$ is located between the two curves of near-field and far-field formulations at large wave frequencies.

4.2 Floating Production Storage Offloading (FPSO) unit

The second example concerns a generic form of FPSO with global length ($L = 300\,\text{m}$), beam ($B = 50\,\text{m}$) and draft ($D = 25\,\text{m}$). The main part (between the stations 25 m and 275 m from the stern) of FPSO is of box shape while the fore part is a circular cylinder and the aft part linearly reduced both in width and in draft, such that the stern has a width and draft equal to 30 and 15 m, respectively. The mesh of the FPSO with 503 panels on one half of the hull and a control surface of box shape ($L_c \times B_c \times D_c = 320 \times 70 \times 30$) are illustrated in Fig. 3. The hull mesh is globally uniform, except for panels close to sharp corners and those touching the waterline whose size is halved. The size of the panels on the control surface varies in

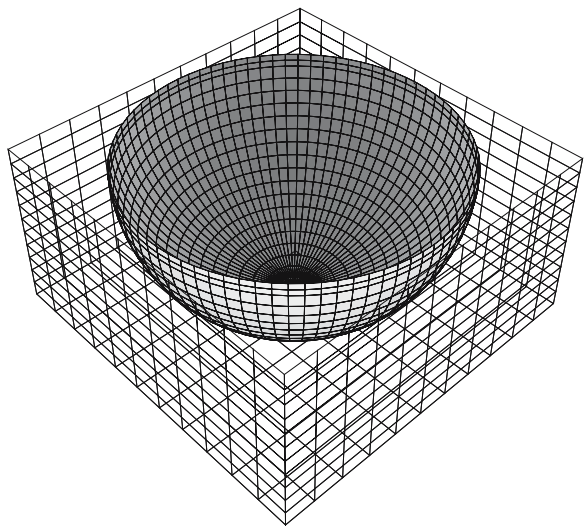

Fig. 1 Mesh of hemisphere and control surface

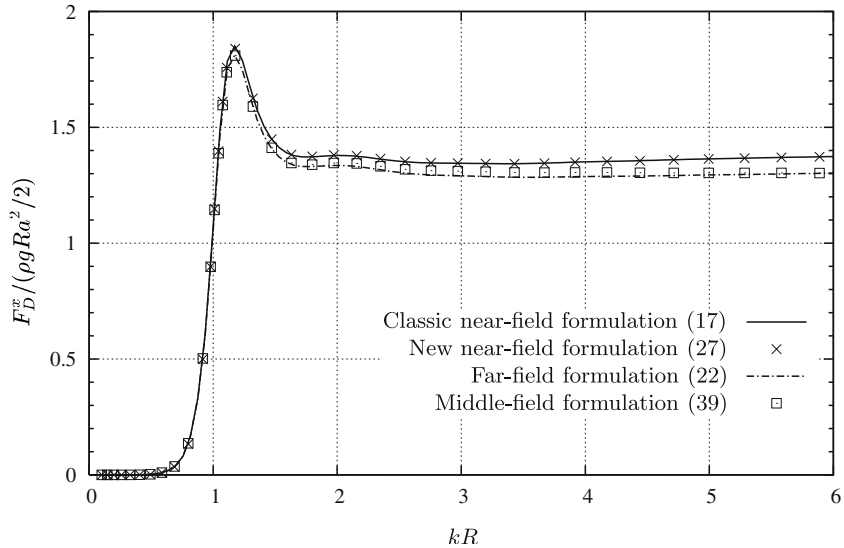

Fig. 2 Drift forces F_D^x on the hemisphere computed with different formulations

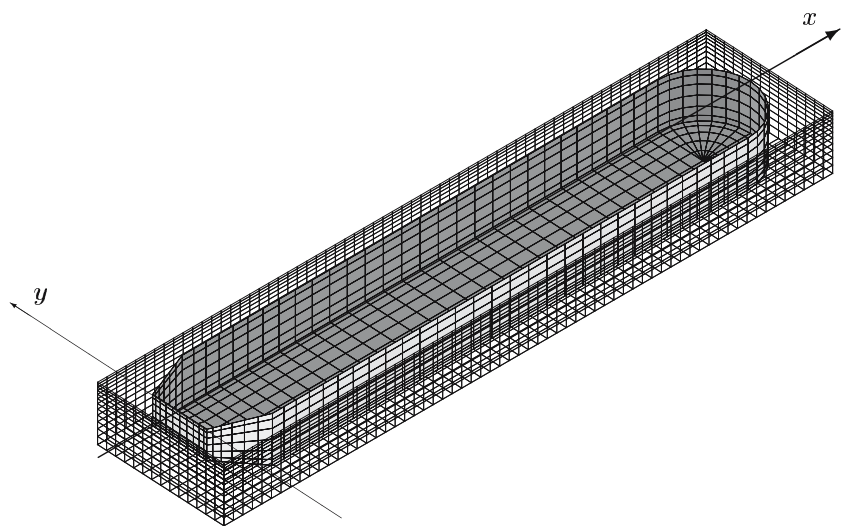

Fig. 3 Mesh of FPSO and control surface

the vertical direction following their position with respect to the free surface. Closer to the free surface, the panel size becomes smaller. The FPSO is freely floating in regular waves. The radii of gyration are 20, 60 and 60 m for the rotational modes in roll, pitch and yaw, respectively. The center of gravity is vertically aligned with the center of buoyancy at the position 151.5 m from the stern and 5 m below the mean free surface.

Three meshes composed of 503, 2012 and 8048 flat panels on one half of the hull are generated. The coarse mesh (2×503 panels) is presented in Fig. 3. Subdividing each panel in the coarse mesh into four produces a finer mesh with 2×2012 panels. The finest mesh (2×8048 panels) is then generated by subdividing each panel in the coarse mesh into 16 smaller parts. Particular attention is paid in the fore part of FPSO where the coordinates of intermediate nodes are calculated on the circular cylinder. All three meshes are used in the solution of wave diffraction and radiation. The linear motion RAOs of surge, sway and heave in an oblique wave of heading $\beta = 165°$ (being measured along the positive direction of the x-axis) are

depicted in Fig. 4 against wave frequencies ω in rad/s. The surge, sway and heave RAOs obtained by using the coarse mesh are presented by the dotted, dot-dashed and solid lines, respectively. The RAOs obtained by using the finer and finest meshes are presented by crosses and squares, respectively. It is observed that any noticeable difference cannot be found in the figure since the results from the three meshes are very close.

In the computation of second-order drift loads, the near-field (27, 28), middle-field (39–41) and far-field formulations (22–24) are used and results are compared. An oblique wave of heading $\beta = 165°$ is considered. The nondimensional drift forces $F_D^x/(\rho g L a^2/2)$ and $F_D^y/(\rho g L a^2/2)$ and drift moment $M_D^z/(\rho g L^2 a^2/2)$ with $L = 300\,\text{m}$ are depicted against the wave frequency (ω) in Figs. 5, 6 and 7, respectively. The results using the near-field formulations are represented by the dotted, dot-dashed and solid lines for the coarse (NF_1), finer (NF_2) and finest (NF_3) meshes, respectively. The results using the middle-field formulation (MF) are shown by circles (coarse mesh), crosses (finer mesh) and squares (finest mesh). The results generated by the far-field formulation (FF) represented by the dotted (coarse mesh), dot-dashed (finer mesh) and solid (finest mesh) lines are indistinguishable from those of the middle-field formulation. For the drift force F_D^x presented in Fig. 5, the results from three meshes and three formulations are very close to each other. However, this is not the case for the drift forces F_D^y presented in Fig. 6 or moments M_D^z in Fig. 7. The curves associated with the near-field formulation are separated for $\omega > 0.50\,\text{rad/s}$. This shows that the results using the near-field formulation are not convergent over the larger part of the wave-frequency range. On the other hand, the results for F_D^y obtained by the far-field formulation (dotted, dot-dashed and solid lines) are indistinguishable over the whole range of the wave frequency. The results for M_D^z from three meshes present some difference at large wave frequencies but are well convergent—the results of the finer and the finest meshes are very close to each other. The same feature is observed for the results associated with the middle-field formulation (circles, crosses and squares). Furthermore, the results of the middle-field formulation are in excellent agreement with those of the far-field formulation.

In the numerical computation of wave-drift loads by using the near-field formulation (27, 28), the tangential fluid velocities are singular at sharp corners of the hull. The global effect of singularities in the velocity field depends not only on the mesh finesse close to the corners but also on the wave heading relative to the corners: more effect on the weather side than on the lee side. In the heading of oblique waves ($\beta = 165°$), the sharp corners where the normal vector has an x-component are on the lee side of waves so that numerical errors are relatively small for surge forces. Numerical experience indicates also that the

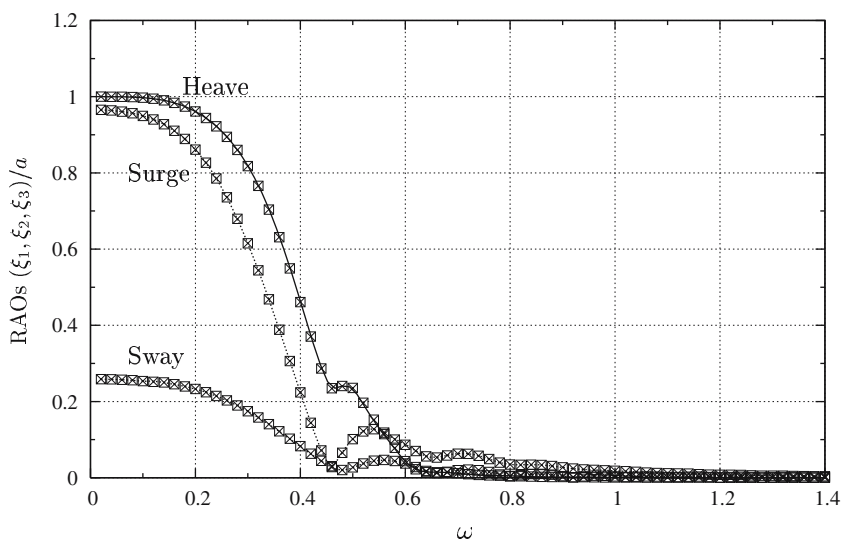

Fig. 4 RAOs of surge, sway and heave in oblique waves ($\beta = 165°$)

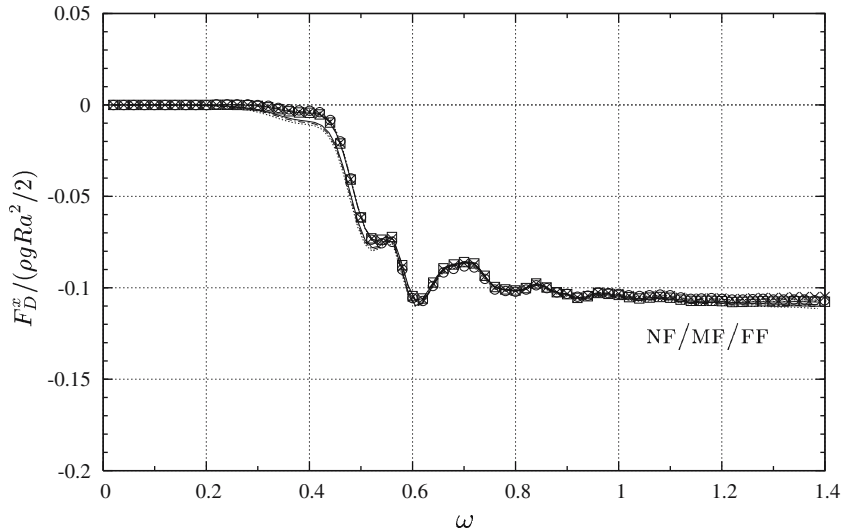

Fig. 5 Drift forces F_D^x on the FPSO in oblique waves ($\beta = 165°$)

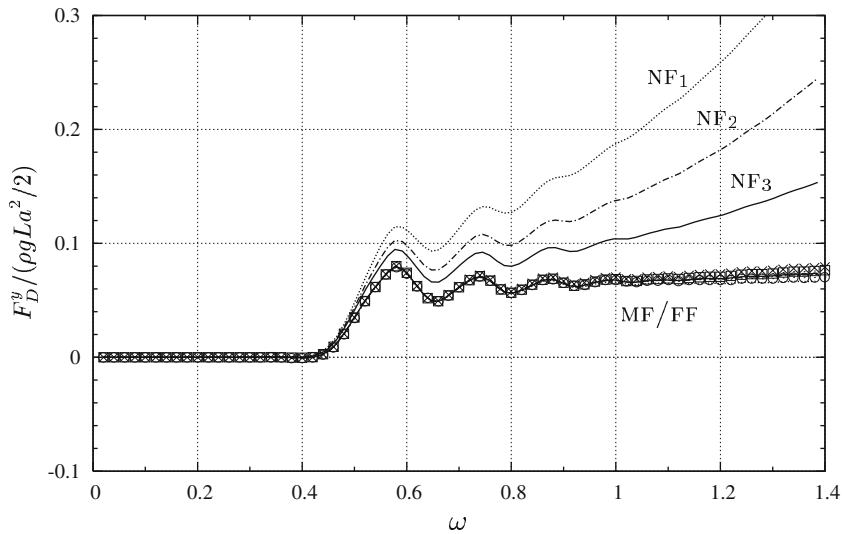

Fig. 6 Drift forces F_D^y on the FPSO in oblique waves ($\beta = 165°$)

surge forces in head/following waves as well as the sway forces in beam waves have better precision that those in oblique waves. In particular, the sway forces and yaw moments are relatively much more affected in slight oblique waves with a heading close to 0° or 180°.

4.3 Two bodies in side-by-side position

We consider now the case of a Wigley hull placed side-by-side with a barge, presented in [16]. Both vessels have dimensions ($L \times B \times T = 2 \times 0.3 \times 0.125$) in meter and are set in beam waves with the two separation distances ($S_1 = 1.097$ and $S_2 = 1.797$) between the two centerlines of the vessels. The case of $S_1 = 1.097$ is considered here. The mesh of the two vessels is represented in Fig. 8 where two separate control surfaces surrounding the two vessels are illustrated, together with the vessels' mesh. The drift loads in the beam

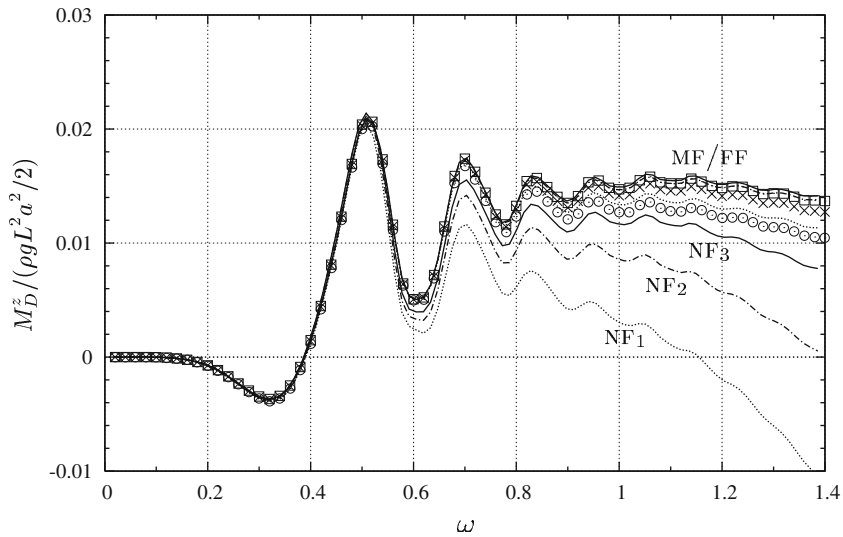

Fig. 7 Drift moments M_D^z on the FPSO in oblique waves ($\beta = 165°$)

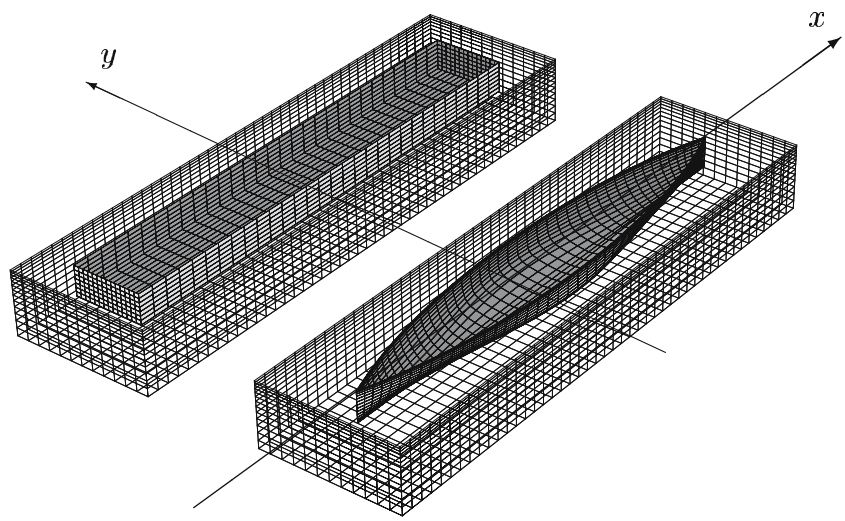

Fig. 8 Mesh of 2 side-by-side vessels and control surfaces

sea with the Wigley hull on the weather side are computed by using both the near-field (dashed lines) and middle-field formulation (solid lines), and compared with the computations (dot-dashed lines) and measurements (squares) in [16]. The two vessels are fixed during the model tests. The sway drift forces $F_D^y/(\rho g L a^2/4)$ on the Wigley hull against the wavenumber $kL/2$ while those on the barge are shown in Fig. 10. In addition, the sway drift forces on the Wigley hull alone (without the barge) and those on the barge alone (without the Wigley hull) are represented by the dotted lines. It can be seen in Figs. 9 and 10 that the numerical results from the different methods are in good agreement and with measurements, even those around $kL/2 \approx 4.7$ where the largest values appear. Note that the numerical results using the near-field formulation in [16] are very close to the present results of sway drift forces in beam sea. This confirms the general remark on numerical results that sway-drift forces in beam waves are relatively less affected by the singularities present in the velocity field at sharp corners, even less sensible in the present case when the Wigley hull with a relatively smoother surface is placed on the weather side of the incoming waves.

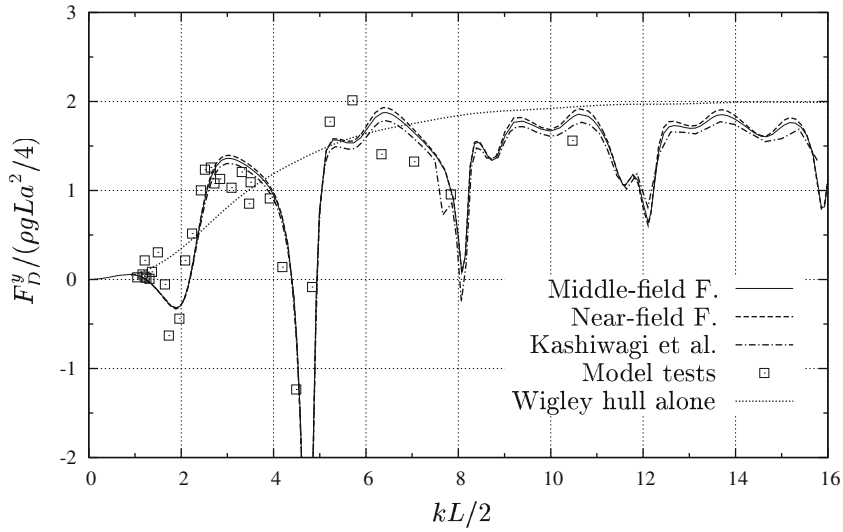

Fig. 9 Drift load F_D^y on the Wigley hull in beam sea ($\beta = 90°$)

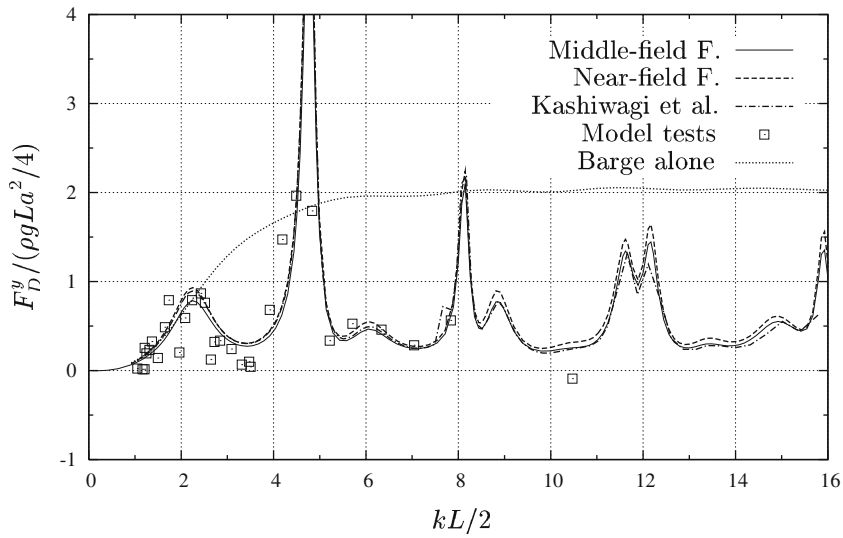

Fig. 10 Drift load F_D^y on the barge in beam sea ($\beta = 90°$)

A slight shift of the wavenumber at which the numerical results present a peak compared to the experimental measurements is observed. The peaks at $kL/2 \approx 4.7, 8, 12, 16$ are associated with large resonant wave kinematics of sloshing type due to the interaction between two bodies. To model the dissipative effect in a real fluid, an additional term representing linear damping is introduced in [17] in the boundary condition over the area of the free surface between the bodies. The method of introducing linear dissipation is indeed effective and provides numerical results very close to those of model tests.

It is remarkable that the sway drift force on the Wigley hull on the weather side of beam waves becomes large negative around $kL/2 \approx 4.7$, while the force on the barge (on the lee side) keeps the same sign and with large values. The sum of the forces on the two vessels remains positive in the whole range of wave frequency. This shows that the important interaction between two bodies creates large repulsion forces between them. At large wave frequencies, the barge on the lee side withstands less forces than those when

it is alone due to the screen effect of the Wigley hull on the weather side. At the limit of infinity frequency, the drift forces on the barge should be nil while those on the Wigley hull tend to the value ($\rho g L a^2/2$) when it stands alone in beam waves.

5 Discussions and conclusions

Starting with the classical near-field formulation (17, 18), we have developed new formulations to evaluate second-order wave loads contributed by the first-order wave field and a body's responses. In particular, the wave-drift forces in the horizontal directions and moments about the vertical axis are expressed by the middle-field formulation (39–41) written *only* on a control surface at a distance from the hull and its intersection with the mean free surface. Its equivalence to the classical far-field formulation (22–24), when the control surface is moved to infinity, demonstrates formally the connection between the near-field and far-field formulations. This equivalence is valid for wall-sided bodies as well as for non-wall-sided bodies. In the near-field formulation [5] for the moments (18), the last term associated with body translation **T** is the moment with respect to the space-fixed reference point resulting from the first-order dynamic load applied to the instantaneous reference point (body-fixed) which is moved due to body translation. This term was omitted in [1, 4] as well as in [6] as it is understood that the moment is evaluated with respect to the body-fixed reference point. In other words, the equivalent far-field formulation must be increased by one term of the same magnitude but with opposite sign, if we define the moments as ones applied to the body-fixed reference point.

Numerical results on the hemisphere confirm the equivalence between the new near-field formulation (27, 28) and the classical one (17, 18), that between the far-field and middle-field formulations, and that between the near-field and far-field formulations. The convergent tests of FPSO with the coarse (2×503), finer (2×2012) and finest (2×8048) meshes show that the results obtained by the near-field formulation for sway-drift forces and yaw moments converge slowly. The method using a higher-order description of hull geometry (B-spline patches, for example) has been expected to give better accurate results than the lower-order method (constant panels) as one developed in [18]. However, the higher-order method is more sensitive to the singularities which are present in the velocity field at sharp corners, as stated in [9]. This sensitivity is manifested when the tangential fluid velocity is computed by (8) as in the evaluation of the mean pressure. As a result, the wave-drift load converges slowly or in the worst cases, it may be non-convergent. On the other hand, the middle-field formulation yields results showing very good convergence that are in excellent agreement with those obtained by the far-field formulation. Furthermore, the middle-field formulation is applied to the case of two bodies. A good agreement with numerical results from other methods and with experimental measurements confirms the important advantages of this new formulation.

Since the middle-field formulation involves wave fields (potentials and velocities) at a distance from the body where there are no singularities, the only condition on the discretization is the correct representation of the wave fields which depend on the body form and wave conditions. In general, the control surface at a distance of 3–5 panels' size from the hull and with a finesse equivalent to that of the body hull gives already good results. A finer mesh close to the free surface is needed for large-frequency waves. On the other hand, the form of the control surface is arbitrary. It can be a parallelepiped box or a semi-ellipsoidal surface. Furthermore, the representation of wave fields over the control surface can be of lower order as the body mesh or otherwise of higher order such as a B-spline, and generated automatically. Since the computation of the wave fields after having obtained first-order solutions is quite efficient, the increase of CPU time is small and comparable to that of the near-field formulation.

The extension to the evaluation of vertical drift forces and moments around the horizontal axes follows directly from expression (37, 38); besides, the additional terms ($\mathbf{F}_S, \mathbf{M}_S$) presented in [6] due to the variation of first-order hydrostatic load are easy to compute. One remaining integral along the waterline and one

over the part of free surface between the control surface and the hull are present in (37, 38). The numerical accuracy of the wave elevation along the waterline and the gradient of the velocity potential at the free surface is relatively good and much better than that of the gradient of the velocity potential on the hull. It is then expected that the *extended* middle-field formulation (37, 38) gives results that converge better than the classical or new near-field formulations.

The second-order oscillatory loads include the low-frequency and high-frequency components taking place at a frequency equal to the difference and sum of the wave frequencies, respectively. These oscillatory loads are composed of one part depending on first-order quantities and another part contributed by the second-order wave field. For the first part, the near-field formulation (17, 18) has been considered as the only way to proceed, unlike the constant drift load for which the far-field formulation is available as well. The numerical burden of poor convergence embedded in the near-field formulation manifests itself again. Now, we have the new general formulation (35, 36) at our disposal which should provide a good alternative for the accurate computation of second-order oscillatory wave loads.

Considering the horizontal low-frequency forces and moments about the vertical axis, the waterline integral in (35, 36), as well as the second term in the free surface integral, disappear. The additional integrals on the hull and over the free surface are proportional to the difference of the wave frequencies. Furthermore, if the body's motion is small ($\mathbf{X} \approx 0$) in waves of small period, the integral over the hull surface is negligible. The integral over the part of free surface can be evaluated easily and accurately since the velocity potentials are not evaluated at the body surface. Thus, it is envisioned that the *extended* middle-field formulation (35, 36) provides a robust method for evaluating the low-frequency horizontal forces and moments about the vertical axis.

Acknowledgements The author would like to thank Professors Dai and Duan from Harbin Engineering University (China) for their comments on the subject and Professor Molin from Ecole Centrale de Marseille (France) for some recent discussions on second-order wave loads. Professor Kashiwagi from Kyushu University (Japan) kindly provided the digital data of his numerical and experimental results.

Appendix A: Variants of Stokes's theorem

Let S be a pierce of a surface with boundary curve Γ. The normal vector $\mathbf{n}$ at a point $\mathbf{r} = (x, y, z)$ is directed towards the positive side of S while the boundary curve Γ is oriented such that it is described *counter-clockwise* about the normal vectors. The unit vector $\mathbf{t}$ along Γ is tangent to Γ in the positive orientation, as illustrated in Fig. 11. The usual Stokes theorem applied to a scalar function $U(x, y, z)$ is given in [19, p. 543] as:

$$\iint_S \mathrm{d}s\, \mathbf{n} \wedge (\nabla U) = \oint_\Gamma \mathrm{d}\ell\, \mathbf{t}\, U \tag{42}$$

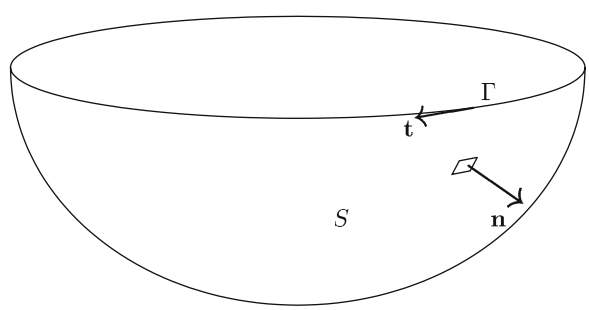

Fig. 11 Definition of (S, Γ) and $(\mathbf{n}, \mathbf{t})$ in Stokes's theorem

and that applied to a vector function $\mathbf{u}$ reads

$$\iint_S \mathrm{d}s\, \mathbf{n}\cdot(\nabla\wedge\mathbf{u}) = \oint_\Gamma \mathrm{d}\ell\, \mathbf{t}\cdot\mathbf{u}. \tag{43}$$

Now, we suppose

$$\mathbf{u} = \mathbf{A}\wedge\mathbf{B}$$

with $\mathbf{B}$ an *arbitrary* vector of non-zero *constant* value. The right-hand side of (43) can then be written as:

$$\oint_\Gamma \mathrm{d}\ell\, \mathbf{t}\cdot\mathbf{u} = \left(\oint_\Gamma \mathrm{d}\ell\, \mathbf{t}\wedge\mathbf{A}\right)\cdot\mathbf{B}, \tag{44}$$

since $(\mathbf{A}\wedge\mathbf{B})\cdot\mathbf{t} = (\mathbf{t}\wedge\mathbf{A})\cdot\mathbf{B}$. On the left-hand side of (43) we have

$$(\nabla\wedge\mathbf{u})\cdot\mathbf{n} = [\nabla\wedge(\mathbf{A}\wedge\mathbf{B})]\cdot\mathbf{n} = [(\mathbf{B}\cdot\nabla)\mathbf{A}]\cdot\mathbf{n} - (\nabla\cdot\mathbf{A})\mathbf{B}\cdot\mathbf{n}. \tag{45}$$

By use of the identity

$$(\nabla\wedge\mathbf{A})\cdot(\mathbf{B}\wedge\mathbf{n}) = [\mathbf{n}\wedge(\nabla\wedge\mathbf{A})]\,\mathbf{B} = [(\mathbf{B}\cdot\nabla)\mathbf{A}]\cdot\mathbf{n} - [(\mathbf{n}\cdot\nabla)\mathbf{A}]\cdot\mathbf{B}, \tag{46}$$

Equation (45) becomes

$$(\nabla\wedge\mathbf{u})\cdot\mathbf{n} = [\mathbf{n}\wedge(\nabla\wedge\mathbf{A}) + (\mathbf{n}\cdot\nabla)\mathbf{A} - (\nabla\cdot\mathbf{A})\mathbf{n}]\cdot\mathbf{B}. \tag{47}$$

Thus, the left-hand side of (43) can be written as:

$$\left(\iint_S \mathrm{d}s\, \mathbf{n}\wedge(\nabla\wedge\mathbf{A}) + (\mathbf{n}\cdot\nabla)\mathbf{A} - (\nabla\cdot\mathbf{A})\mathbf{n}\right)\cdot\mathbf{B}. \tag{48}$$

Since $\mathbf{B}$ is arbitrary, (44) and (48) leads to the first variant of Stokes's theorem:

$$\iint_S \mathrm{d}s\left\{(\nabla\cdot\mathbf{A})\mathbf{n} - \mathbf{n}\wedge(\nabla\wedge\mathbf{A}) - (\mathbf{n}\cdot\nabla)\mathbf{A}\right\} = \oint_\Gamma \mathrm{d}\ell\, \mathbf{A}\wedge\mathbf{t}. \tag{49}$$

Next, we assume

$$\mathbf{u} = \mathbf{A}\wedge(\mathbf{r}\wedge\mathbf{B})$$

with $\mathbf{B}$ again an arbitrary constant vector. Since

$$\mathbf{u}\cdot\mathbf{t} = [\mathbf{A}\wedge(\mathbf{r}\wedge\mathbf{B})]\cdot\mathbf{t} = [\mathbf{r}(\mathbf{B}\cdot\mathbf{A}) - \mathbf{B}(\mathbf{A}\cdot\mathbf{r})]\cdot\mathbf{t} = [(\mathbf{r}\cdot\mathbf{t})\mathbf{A} - (\mathbf{A}\cdot\mathbf{r})\mathbf{t}]\cdot\mathbf{B} = [\mathbf{r}\wedge(\mathbf{A}\wedge\mathbf{t})]\cdot\mathbf{B},$$

the right-hand side of (43) can be written as:

$$\oint_\Gamma \mathrm{d}\ell\, \mathbf{u}\cdot\mathbf{t} = \left(\oint_\Gamma \mathrm{d}\ell\, \mathbf{r}\wedge(\mathbf{A}\wedge\mathbf{t})\right)\cdot\mathbf{B} \tag{50}$$

while the left-hand side

$$\begin{aligned}(\nabla\wedge\mathbf{u})\cdot\mathbf{n} &= \Big\{\nabla\wedge\big[\mathbf{A}\wedge(\mathbf{r}\wedge\mathbf{B})\big]\Big\}\cdot\mathbf{n}\\ &= \Big\{\big[(\mathbf{r}\wedge\mathbf{B})\cdot\nabla\big]\mathbf{A} - (\mathbf{A}\cdot\nabla)(\mathbf{r}\wedge\mathbf{B}) + \mathbf{A}\big[\nabla\cdot(\mathbf{r}\wedge\mathbf{B})\big] - (\mathbf{r}\wedge\mathbf{B})(\nabla\cdot\mathbf{A})\Big\}\cdot\mathbf{n}\end{aligned} \tag{51}$$

obtained by using the identity given in [19, p. 538] reads:

$$\nabla\wedge(\mathbf{A}\wedge\mathbf{Y}) = (\mathbf{Y}\cdot\nabla)\mathbf{A} - (\mathbf{A}\cdot\nabla)\mathbf{Y} + \mathbf{A}(\nabla\cdot\mathbf{Y}) - \mathbf{Y}(\nabla\cdot\mathbf{A})$$

with $\mathbf{Y} = \mathbf{r}\wedge\mathbf{B}$. Furthermore, considering the identities

$$\mathbf{X}\cdot(\mathbf{Y}\wedge\mathbf{n}) = \mathbf{Y}\cdot(\mathbf{n}\wedge\mathbf{X}) \quad \text{with} \quad \mathbf{X} = \nabla\wedge\mathbf{A},$$
$$\mathbf{n}\wedge\mathbf{X} = \nabla(\mathbf{A}\cdot\mathbf{n}) - (\mathbf{n}\cdot\nabla)\mathbf{A} \quad \text{and} \quad \mathbf{Y}\cdot[\nabla(\mathbf{A}\cdot\mathbf{n})] = [(\mathbf{Y}\cdot\nabla)\mathbf{A}]\cdot\mathbf{n},$$

we have

$$(\nabla\wedge\mathbf{A})\cdot\big[(\mathbf{r}\wedge\mathbf{B})\wedge\mathbf{n}\big] = \Big\{\big[(\mathbf{r}\wedge\mathbf{B})\cdot\nabla\big]\mathbf{A}\Big\}\cdot\mathbf{n} - \Big\{\big[(\mathbf{n}\cdot\nabla)\mathbf{A}\big]\wedge\mathbf{r}\Big\}\cdot\mathbf{B},$$

together with

$$(\nabla\wedge\mathbf{A})\cdot\big[(\mathbf{r}\wedge\mathbf{B})\wedge\mathbf{n}\big]=(\mathbf{r}\wedge\mathbf{B})\cdot\big[\mathbf{n}\wedge(\nabla\wedge\mathbf{A})\big]=\Big\{-\mathbf{r}\wedge\big[\mathbf{n}\wedge(\nabla\wedge\mathbf{A})\big]\Big\}\cdot\mathbf{B}$$

directly derived from (46), so that

$$\Big\{\big[(\mathbf{r}\wedge\mathbf{B})\cdot\nabla\big]\mathbf{A}\Big\}\cdot\mathbf{n}=\Big\{-\mathbf{r}\wedge\big[\mathbf{n}\wedge(\nabla\wedge\mathbf{A})\big]+\big[(\mathbf{n}\cdot\nabla)\mathbf{A}\big]\wedge\mathbf{r}\Big\}\cdot\mathbf{B}.$$

Other terms in (51) are

$$-\big[(\mathbf{A}\cdot\nabla)(\mathbf{r}\wedge\mathbf{B})\big]\cdot\mathbf{n}=-(\mathbf{A}\wedge\mathbf{B})\cdot\mathbf{n}=(\mathbf{A}\wedge\mathbf{n})\cdot\mathbf{B},$$

$$\Big\{\mathbf{A}\big[\nabla\cdot(\mathbf{r}\wedge\mathbf{B})\big]\Big\}\cdot\mathbf{n}=\{\mathbf{A}[0]\}\cdot\mathbf{n}=0,$$

$$-\big[(\mathbf{r}\wedge\mathbf{B})(\nabla\cdot\mathbf{A})\big]\cdot\mathbf{n}=\big[(\nabla\cdot\mathbf{A})(\mathbf{r}\wedge\mathbf{n})\big]\cdot\mathbf{B},$$

so that the left-hand side of (43) is:

$$\left(\iint_S \mathrm{d}s\,(\nabla\cdot\mathbf{A})(\mathbf{r}\wedge\mathbf{n})+\mathbf{A}\wedge\mathbf{n}-\mathbf{r}\wedge\big[\mathbf{n}\wedge(\nabla\wedge\mathbf{A})\big]-\mathbf{r}\wedge\big[(\mathbf{n}\cdot\nabla)\mathbf{A}\big]\right)\cdot\mathbf{B}. \tag{52}$$

Since $\mathbf{B}$ is arbitrary, Eqs. 50 and 52 yield the second variant of Stokes's theorem:

$$\iint_S \mathrm{d}s\left\{(\nabla\cdot\mathbf{A})(\mathbf{r}\wedge\mathbf{n})+\mathbf{A}\wedge\mathbf{n}-\mathbf{r}\wedge\big[\mathbf{n}\wedge(\nabla\wedge\mathbf{A})\big]-\mathbf{r}\wedge\big[(\mathbf{n}\cdot\nabla)\mathbf{A}\big]\right\}=\oint_\Gamma \mathrm{d}\ell\,\mathbf{r}\wedge(\mathbf{A}\wedge\mathbf{t}). \tag{53}$$

The development of these two variants of Stokes's theorem can be found as Equations (1.3.5) and (1.3.13) in [10].

Appendix B: Application of the variants of Stokes's theorem

Considering the vector $\mathbf{A}=\Phi_t\mathbf{X}$ with $\mathbf{X}=\mathbf{T}+\mathbf{R}\wedge\mathbf{r}$, we have

$$\nabla\cdot\mathbf{A}=\Phi_t\nabla\cdot\mathbf{X}+\mathbf{X}\cdot\nabla\Phi_t=\mathbf{X}\cdot\nabla\Phi_t,$$

since $\nabla\cdot\mathbf{X}=0$. By making use of the first variant of Stokes's theorem (49), the hull integral (17) involving the second term of the integrand can be written as

$$\iint_H \mathrm{d}s\left\{(\mathbf{X}\cdot\nabla\Phi_t)\mathbf{n}-\mathbf{n}\wedge[\nabla\wedge(\Phi_t\mathbf{X})]-(\mathbf{n}\cdot\nabla)(\Phi_t\mathbf{X})\right\}=\oint_\Gamma \mathrm{d}\ell\,(\Phi_t\mathbf{X})\wedge\mathbf{t}. \tag{54}$$

Some algebraic calculations are necessary and listed in the following:

$$\begin{aligned}\mathbf{n}\wedge[\nabla\wedge(\Phi_t\mathbf{X})]&=\mathbf{n}\wedge[\Phi_t(\nabla\wedge\mathbf{X})+\nabla\Phi_t\wedge\mathbf{X}]\\&=\mathbf{n}\wedge[2\Phi_t\mathbf{R}+\nabla\Phi_t\wedge\mathbf{X}]\\&=-2\Phi_t\mathbf{R}\wedge\mathbf{n}+\nabla\Phi_t(\mathbf{X}\cdot\mathbf{n})-\mathbf{X}(\nabla\Phi_t\cdot\mathbf{n})\\(\mathbf{n}\cdot\nabla)(\Phi_t\mathbf{X})&=\mathbf{X}(\nabla\Phi_t\cdot\mathbf{n})+\Phi_t(\mathbf{n}\cdot\nabla)\mathbf{X}\\&=\mathbf{X}(\nabla\Phi_t\cdot\mathbf{n})+\Phi_t(\mathbf{R}\wedge\mathbf{n}),\end{aligned}$$

in which we have used $\nabla\wedge\mathbf{X}=2\mathbf{R}$ and $(\mathbf{n}\cdot\nabla)\mathbf{X}=\mathbf{R}\wedge\mathbf{n}$ so that:

$$\iint_H \mathrm{d}s\left\{(\mathbf{X}\cdot\nabla\Phi_t)\mathbf{n}+\mathbf{R}\wedge(\Phi_t\mathbf{n})-\nabla\Phi_t(\mathbf{X}\cdot\mathbf{n})\right\}=-g\oint_\Gamma \mathrm{d}\ell\,\eta(\mathbf{X}\wedge\mathbf{t}), \tag{55}$$

where we have used $\Phi_t=-g\eta$ from (10) along the waterline.

At the waterline, the tangential vector $\mathbf{t} = (t_1, t_2) = (\bar{n}_2, -\bar{n}_1)$ where $\bar{n}_1$ and $\bar{n}_2$ are the horizontal components of the normal vector *contained* on the mean free surface $\bar{\mathbf{n}} = (\bar{n}_1, \bar{n}_2, 0)$ as illustrated in Fig. 12, we have:

$$\oint_\Gamma \mathrm{d}\ell\, \eta(\mathbf{X} \wedge \mathbf{t}) = \oint_\Gamma \mathrm{d}\ell\, \eta\big[\zeta_3 \bar{\mathbf{n}} - (\mathbf{X} \cdot \bar{\mathbf{n}})\mathbf{k}\big] \tag{56}$$

Introducing (56) into (55), we obtain

$$\iint_H \mathrm{d}s \left\{ (\mathbf{X} \cdot \nabla\Phi_t)\mathbf{n} + \mathbf{R} \wedge (\Phi_t \mathbf{n}) - \nabla\Phi_t (\mathbf{X} \cdot \mathbf{n}) \right\} = -g \oint_\Gamma \mathrm{d}\ell\, \eta\big[\zeta_3 \bar{\mathbf{n}} - (\mathbf{X} \cdot \bar{\mathbf{n}})\mathbf{k}\big]. \tag{57}$$

In a similar way, we apply second variant of Stokes's theorem (53) to the second term of the hull integral (18):

$$\begin{aligned} &\iint_H \mathrm{d}s \left\{ (\mathbf{X} \cdot \nabla\Phi_t)(\mathbf{r} \wedge \mathbf{n}) + (\Phi_t \mathbf{X}) \wedge \mathbf{n} - \mathbf{r} \wedge \big\{ \mathbf{n} \wedge [\nabla \wedge (\Phi_t \mathbf{X})] \big\} - \mathbf{r} \wedge [(\mathbf{n} \cdot \nabla)(\Phi_t \mathbf{X})] \right\} \\ &\quad = \oint_\Gamma \mathrm{d}\ell\, \mathbf{r} \wedge [(\Phi_t \mathbf{X}) \wedge \mathbf{t}]. \end{aligned} \tag{58}$$

Some calculations are listed here:

$$\begin{aligned} (\Phi_t \mathbf{X}) \wedge \mathbf{n} &= \mathbf{T} \wedge (\Phi_t \mathbf{n}) + \Phi_t [(\mathbf{R} \wedge \mathbf{r}) \wedge \mathbf{n}] \\ &= \mathbf{T} \wedge (\Phi_t \mathbf{n}) + \Phi_t [\mathbf{r}(\mathbf{R} \cdot \mathbf{n}) - \mathbf{R}(\mathbf{r} \cdot \mathbf{n})], \end{aligned}$$

$$\begin{aligned} \mathbf{r} \wedge \big\{ \mathbf{n} \wedge [\nabla \wedge (\Phi_t \mathbf{X})] \big\} &= \mathbf{r} \wedge \big\{ -2\Phi_t \mathbf{R} \wedge \mathbf{n} + \nabla\Phi_t (\mathbf{X} \cdot \mathbf{n}) - \mathbf{X}(\nabla\Phi_t \cdot \mathbf{n}) \big\} \\ &= -2\Phi_t [\mathbf{r} \wedge (\mathbf{R} \wedge \mathbf{n})] + (\mathbf{r} \wedge \nabla\Phi_t)(\mathbf{X} \cdot \mathbf{n}) - (\mathbf{r} \wedge \mathbf{X})(\nabla\Phi_t \cdot \mathbf{n}), \end{aligned}$$

$$\begin{aligned} \mathbf{r} \wedge [(\mathbf{n} \cdot \nabla)(\Phi_t \mathbf{X})] &= (\mathbf{r} \wedge \mathbf{X}) \cdot (\nabla\Phi_t \cdot \mathbf{n}) + \Phi_t [\mathbf{r} \wedge (\mathbf{R} \wedge \mathbf{n})], \\ \mathbf{r} \wedge [(\Phi_t \mathbf{X}) \wedge \mathbf{t}] &= \Phi_t [\mathbf{r} \wedge (\mathbf{X} \wedge \mathbf{t})] \\ &= \Phi_t [\zeta_3 (\mathbf{r} \wedge \bar{\mathbf{n}}) - (\mathbf{X} \cdot \bar{\mathbf{n}})(\mathbf{r} \wedge \mathbf{k})], \end{aligned}$$

so that:

$$\begin{aligned} &\iint_H \mathrm{d}s \left\{ (\mathbf{X} \cdot \nabla\Phi_t)(\mathbf{r} \wedge \mathbf{n}) + \mathbf{T} \wedge (\Phi_t \mathbf{n}) + \mathbf{R} \wedge [\Phi_t (\mathbf{r} \wedge \mathbf{n})] - (\mathbf{r} \wedge \nabla\Phi_t)(\mathbf{X} \cdot \mathbf{n}) \right\} \\ &\quad = -g \oint_\Gamma \mathrm{d}\ell\, \eta\big[\zeta_3 (\mathbf{r} \wedge \bar{\mathbf{n}}) - (\mathbf{X} \cdot \bar{\mathbf{n}})(\mathbf{r} \wedge \mathbf{k})\big] \end{aligned} \tag{59}$$

with $\bar{\mathbf{n}}$ the normal vector along the waterline on the mean free surface orthogonal to the tangential vector $\mathbf{t}$.

It is worth noting that the unit normal vector $\bar{\mathbf{n}}$ along the waterline defined on the mean free surface is equal to the normal vector $\mathbf{n}$ on the hull of a wall-sided body which intersects vertically the mean free

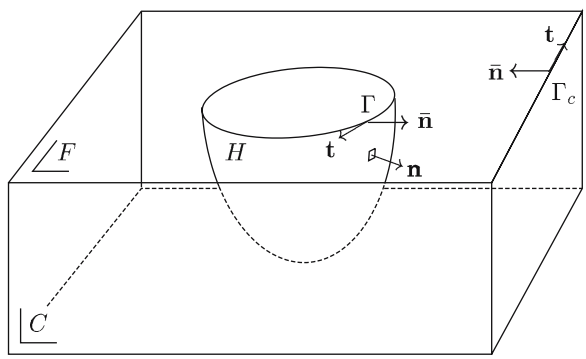

Fig. 12 Definition of control surfaces and different unit vectors

surface. In the general case, if the angle between the normal vector $\mathbf{n}$ on the hull and the mean free surface is denoted by γ, we have the relation:

$$\bar{\mathbf{n}} = (\bar{n}_1, \bar{n}_2, 0) = (n_1, n_2, 0)/\sqrt{n_1^2 + n_2^2} = (n_1, n_2, 0)/\sqrt{1 - n_3^2} = (n_1, n_2, 0)/|\cos\gamma| \tag{60}$$

with the normal vector $\mathbf{n} = (n_1, n_2, n_3)$ on the hull. For a wall-sided body, $\gamma = 0$, so that $\bar{\mathbf{n}} = \mathbf{n}$ from (60).

Appendix C: Application of Gauss's theorem

Let D be a domain of space with boundary surface S with the normal $\mathbf{n}$ to S being oriented *inwards*. Gauss's theorem in [19, p. 541] applied to a continuous scalar function $U(x, y, z)$ in D gives :

$$\iint_S \mathrm{d}s\, \mathbf{n}\, U = -\iiint_D \mathrm{d}v\, \nabla U \tag{61}$$

or to a vector function $\mathbf{u}$

$$\iint_S \mathrm{d}s\, \mathbf{n}\cdot\mathbf{u} = -\iiint_D \mathrm{d}v\, \nabla\cdot\mathbf{u} \quad \text{and} \quad \iint_S \mathrm{d}s\, \mathbf{n}\wedge\mathbf{u} = -\iiint_D \mathrm{d}v\, \nabla\wedge\mathbf{u}. \tag{62}$$

Substituting U for $\nabla\Phi\nabla\Phi$ in the first formula of (61) and using the identity $\nabla U = 2(\nabla\Phi\nabla)\nabla\Phi$, we have :

$$\iint_S \mathrm{d}s\, (\nabla\Phi\cdot\nabla\Phi)\mathbf{n} = -2\iiint_D \mathrm{d}v\, (\nabla\Phi\cdot\nabla)\nabla\Phi. \tag{63}$$

The integrand on the right-hand side of (63) can be developed as:

$$(\nabla\Phi\cdot\nabla)\nabla\Phi = (\nabla\Phi\cdot\nabla\Phi_x)\mathbf{i} + (\nabla\Phi\cdot\nabla\Phi_y)\mathbf{j} + (\nabla\Phi\cdot\nabla\Phi_z)\mathbf{k} = \nabla\cdot(\nabla\Phi\Phi_x)\mathbf{i} + \nabla\cdot(\nabla\Phi\Phi_y)\mathbf{j} + \nabla\cdot(\nabla\Phi\Phi_z)\mathbf{k}.$$

The first formula of (62) gives

$$\begin{aligned}&\iiint_D \mathrm{d}v\big[\nabla\cdot(\nabla\Phi\Phi_x)\mathbf{i} + \nabla\cdot(\nabla\Phi\Phi_y)\mathbf{j} + \nabla\cdot(\nabla\Phi\Phi_z)\mathbf{k}\big]\\ &\quad = -\iint_S \mathrm{d}s\, \mathbf{n}\cdot\big[(\nabla\Phi\Phi_x)\mathbf{i} + (\nabla\Phi\Phi_y)\mathbf{j} + (\nabla\Phi\Phi_z)\mathbf{k}\big] = -\iint_S \mathrm{d}s\, (\mathbf{n}\cdot\nabla\Phi)\nabla\Phi = -\iint_S \mathrm{d}s\, \Phi_n\nabla\Phi,\end{aligned} \tag{64}$$

so that

$$\iint_S \mathrm{d}s\, (\nabla\Phi\cdot\nabla\Phi)\mathbf{n} = 2\iint_S \mathrm{d}s\, \Phi_n\nabla\Phi. \tag{65}$$

In the same way, Gauss's theorem gives

$$\iint_S \mathrm{d}s\, (\nabla\Phi\cdot\nabla\Phi)(\mathbf{r}\wedge\mathbf{n}) = \iint_S \mathrm{d}s\, [(\nabla\Phi\cdot\nabla\Phi)\mathbf{r}]\wedge\mathbf{n} = \iiint_D \mathrm{d}v\, \nabla\wedge[(\nabla\Phi\cdot\nabla\Phi)\mathbf{r}] \tag{66}$$

according to the second formula of (62). The integrand on the right side of (66) can be developed as follows:

$$\begin{aligned}\nabla\wedge[(\nabla\Phi\cdot\nabla\Phi)\mathbf{r}] &= -\mathbf{r}\wedge[\nabla(\nabla\Phi\cdot\nabla\Phi)] = -2\mathbf{r}\wedge[(\nabla\Phi\cdot\nabla)\nabla\Phi] = -2(\nabla\Phi\cdot\nabla)(\mathbf{r}\wedge\nabla\Phi)\\ &= -2\Big\{\nabla\cdot\big[\nabla\Phi(y\Phi_z - z\Phi_y)\big]\mathbf{i} + \nabla\cdot\big[\nabla\Phi(z\Phi_x - x\Phi_z)\big]\mathbf{j} + \nabla\cdot\big[\nabla\Phi(x\Phi_y - y\Phi_x)\big]\mathbf{k}\Big\}.\end{aligned}$$

By use of the first formula of (62), the integral (66) becomes:

$$\begin{aligned}&2\iint_S \mathrm{d}s\, \mathbf{n}\cdot\Big\{\big[\nabla\Phi(y\Phi_z - z\Phi_y)\big]\mathbf{i} + \big[\nabla\Phi(z\Phi_x - x\Phi_z)\big]\mathbf{j} + \big[\nabla\Phi(x\Phi_y - y\Phi_x)\big]\mathbf{k}\Big\}\\ &\quad = 2\iint_S \mathrm{d}s\, (\mathbf{n}\cdot\nabla\Phi)(\mathbf{r}\wedge\nabla\Phi),\end{aligned} \tag{67}$$

so that

$$\iint_S \mathrm{d}s\, (\nabla\Phi\cdot\nabla\Phi)(\mathbf{r}\wedge\mathbf{n}) = 2\iint_S \mathrm{d}s\, \Phi_n(\mathbf{r}\wedge\nabla\Phi). \tag{68}$$

The identity (65) can be found also as [20, Equation 89].

Over the area F of the mean free surface limited by its common boundary Γ with the hull H and its common boundary Γ_c with the control surface C, we can apply the Gauss integral for the plane given in [19, p. 543]:

$$\iint_F \mathrm{d}s\,(\nabla\Phi_t - \Phi_{zt}\mathbf{k})\Phi_t = \iint_F \mathrm{d}s\,(\Phi_{xt}\mathbf{i} + \Phi_{yt}\mathbf{j})\Phi_t = \frac{1}{2}\iint_F \mathrm{d}s\left[\partial_x(\Phi_t\Phi_t)\mathbf{i} + \partial_y(\Phi_t\Phi_t)\mathbf{j}\right]$$
$$= \frac{1}{2}\left(\oint_\Gamma + \oint_{\Gamma_c}\right)(\mathrm{d}y\,\mathbf{i} - \mathrm{d}x\,\mathbf{j})\,(\Phi_t\Phi_t) = -\frac{1}{2}\left(\oint_\Gamma + \oint_{\Gamma_c}\right)\mathrm{d}l\,\bar{\mathbf{n}}(\Phi_t\Phi_t), \tag{69}$$

since $(\mathrm{d}x, \mathrm{d}y) = \mathrm{d}l(\bar{n}_2, -\bar{n}_1)$ along Γ and Γ_c as illustrated in Fig. 12.

In the same way, we have:

$$\iint_F \mathrm{d}s\,\mathbf{r}\wedge(\nabla\Phi_t - \Phi_{zt}\mathbf{k})\Phi_t = -\frac{1}{2}\left(\oint_\Gamma + \oint_{\Gamma_c}\right)\mathrm{d}l\,\mathbf{r}\wedge\bar{\mathbf{n}}(\Phi_t\Phi_t) \tag{70}$$

with $\bar{\mathbf{n}} = (\bar{n}_1, \bar{n}_2, 0)$ being the normal vector along Γ and Γ_c and contained on F.

References

1. Pinkster JA, van Oortmerssen G (1977) Computation of the first- and second-order wave forces on oscillating bodies in regular waves. Proc. 2nd Int. Conf. Num. Ship Hydrodynamics, Berkley, USA, pp 136–156
2. Molin B (1979a) Computations of wave drift forces. Proc. OTC Conf., Houston, USA, paper No. 3627
3. Molin B (1979b) Second-order drift forces upon large bodies in regular waves. Proc. BOSS'79., London, UK, pp 363–370
4. Pinkster JA (1980) Low frequency second order wave exciting forces on floating structures. H. Veenman En Zonen B.V., The Netherlands, Wageningen
5. Ogilvie TF (1983) Second-order hydrodynamic effects on ocean platforms. Proc. Intl Workshop on Ship & Platform Motions, Berkeley, USA, pp 205–265
6. Molin B, Hairault JP (1983) On second-order motion and vertical drift forces for three-dimensional bodies in regular waves. Proc. Intl Workshop on Ship & Platform Motions, Berkeley, USA, pp 344–362
7. Maruo H (1960) The drift of a body floating on waves. J Ship Res 4:1–10
8. Newman JN (1967) The drift force and moment on ships in waves. J Ship Res 11:51–60
9. Newman JN, Lee CH (2001) Boundary-element methods in offshore structure analysis. Proc. 20th Intl Conf. Off. Mech. Arc. Engeng, Rio de Janeiro, Brazil
10. Dai YS (1998) Potential flow theory of ship motions in waves in frequency and time domain (in Chinese). Press of the National Defense Industries, Beijing, China
11. Ferreira MD, Lee CH (1994) Computation of second-order mean wave forces and moments in multibody interaction. Proc. 7th Intl Conf. Behaviour Off. Structures, BOSS'94, Boston, USA, vol 2, pp 303–313
12. Noblesse F (1982) The Green function in the theory of radiation and diffraction of regular waves by a body, J Engg Math 16:137–169
13. Newman JN (1992) The approximation of free-surface Green functions, Wave asymptotics — Proc. F. Ursell Retirement Meeting, Cambridge University Press, pp 107–135
14. Chen XB (1993) Evaluation de la fonction de Green du problème de diffraction/radiation en profondeur d'eau finie — Une nouvelle méthode rapide and précise, Proc. 4e Journées de l'Hydrodynamique, Nantes, France, pp 371–384
15. Guével P (1982) Le problème de diffraction-radiation — Premième partie: Théorèmes fondamentaux. Ecole Supérieure de Mécanique de Nantes, Nantes, France
16. Kashiwagi M, Endo K, Yamaguchi H (2005) Wave drift forces and moments on two ships arranged side by side in waves. J Ocean Eng 32:529–555
17. Chen XB (2004) Hydrodynamics in Offshore and Naval Applications — Part I. Keynote lecture at the 6th Intl Conference on Hydrodynamics, Perth, Australia
18. Chen XB (1988) Etude des réponses du second ordre d'une structure soumise à une houle aléatoire. Ph.D. Thesis, ENSM, Univ. Nantes, Nantes, France
19. Bronshtein IN, Semendyayev KA (1998) Handbook of Mathematics. Springer-Verlag, Berlin, Heidelberg
20. Newman JN (1977) Marine Hydrodynamics. The MIT Press, Cambridge, USA